JOURNAL OF AIRCRAFT
Vol. 44, No. 3, May–June 2007

Engineering Notes

ENGINEERING NOTES are short manuscripts describing new developments or important results of a preliminary nature. These Notes should not exceed 2500 words (where a figure or table counts as 200 words). Following informal review by the Editors, they may be published within a few months of the date of receipt. Style requirements are the same as for regular contributions (see inside back cover).

Comparison of Computational Fluid Dynamics Approaches for Simulating Weapons Bay Flow

R. H. Nichols*
University of Alabama in Birmingham, Birmingham, Alabama 35294
and
Shawn Westmoreland†
Digital Fusion, Inc., Huntsville, Alabama 35806

DOI: 10.2514/1.23067

Introduction

CURRENT and future aircraft weapons platforms use an internal carriage of munitions to reduce the signature of the vehicle. The increase in accuracy of modern munitions has led to a reduction of the size and weight of the weapons. These new munitions are generally noncircular in cross section and include geometrical features such as wings, strakes, or fins to improve their standoff capability and maneuverability. Weapons must be capable of withstanding the acoustic environment of the bay and must exit the bay in a stable orientation to perform their mission. The flowfield inside a weapons bay is unsteady and contains complex large-scale turbulent flow structures. The unsteady nature of the flow in the bay coupled with the lighter and more complicated weapons geometry makes weapons separation much more difficult to predict than for the externally carried heavy circular-geometry weapons of the past.

Several techniques have been successfully used in the weapons separation design process in the past. Semi-empirical methods [1] allow the designer to examine a large design matrix quickly. The semi-empirical methods require aircraft flowfield and weapon freestream aerodynamic information that can be obtained from the wind tunnel or from computational fluid dynamics (CFD). Unsteady time-accurate moving-body CFD can also be used to provide weapons separation simulations, but the time per solution is still too high to allow an entire aircraft/weapon design matrix to be examined with moving body CFD alone. A combination of semi-empirical and CFD methods has been shown to be effective in determining the separation characteristics of a weapon from an aircraft [2–4]. Semi-empirical methods rely on time-averaged flowfields that are generally generated using CFD. These techniques assume that the time-averaged flowfield is sufficient for bay trajectory simulations. Jordan and Denny [5] demonstrated that this may not always be the case. Methods to assess unsteady effects on weapon trajectories and account for the unsteady flowfields need to be developed for semi-empirical methods.

Researchers have been attempting to predict the acoustical environment inside a weapons bay for several years. Rizzetta [6], Suhs [7], and Baysal et al. [8] used the Baldwin–Lomax (BL) [9] algebraic turbulence model in investigations of bay acoustics. These applications represent an early form of hybrid turbulence modeling. The algebraic turbulence model was applied to the flat plate outside of the bay, and no turbulence model was used in the shear layer region of the cavity. This methodology allowed for a reasonable simulation of the incoming boundary layer and allowed the unsteady flow to develop using the laminar viscosity alone. The sound pressure level spectrum was generally overpredicted because there was no turbulent eddy viscosity included in the shear layer over the cavity.

Atwood [10] performed CFD calculations of a store separating from a rectangular bay. The Baldwin–Lomax [9] turbulence model was used on the walls of the bay and the plate. An algebraic turbulence model was applied in the cavity shear layer region. Comparisons with the cavity acoustics were not included in this paper, but a comparison of the trajectory of a missile separating from the bay with and without an autopilot was presented. The computed trajectory of the store was in reasonable agreement with the experimental result.

An unsteady Euler simulation of a fighter aircraft main weapons bay was performed by Welterlen [11]. The time-averaged results for static pressure and velocities in the outer shear layer region above the bay were compared to wind tunnel results and provided relatively good agreement ($\sim$5%) for the conditions shown. The computational acoustic results were not in good agreement with the experimental data.

Tramel and Nichols [12] used a two-equation k–ε Reynolds averaged Navier–Stokes (RANS) turbulence model for a supersonic cavity acoustic application. The time-averaged pressure and overall sound pressure were in reasonable agreement with experimental data. The spectral peaks were predicted at the proper frequencies, but the levels were underpredicted. This was because the turbulence model was providing too much eddy viscosity in the cavity shear layer. Sinha et al. [13] and Arunajatesan et al. [14] investigated a supersonic bay acoustics using a hybrid RANS/LES (large eddy simulation) turbulence model. The time-averaged pressures and overall sound pressure levels were in reasonable agreement with experimental data. The spectral results were not in agreement with the data of [15]. Nichols and Nelson [16] present acoustic results for two RANS models and two hybrid RANS/LES models for a transonic bay. The two RANS models produced similar results and overdamped the unsteady flow. Nichols [17] also investigated the grid and time step sensitivity of three hybrid RANS/LES turbulence models for a transonic bay. All of these hybrid RANS/LES results were in good agreement with the data for the time-averaged pressure, overall sound pressure level, and sound pressure level spectrum.

Rizzetta and Visbal [18] used LES to investigate the acoustics in a simple rectangular cavity having a length to depth ratio of 5:1. The sidewalls of the cavity were not included in the simulation. The grid system contained 2×10^7 points for a simulation of $M = 1.19$ flow at a Reynolds number of 2×10^5 based on cavity length. Rizzetta and Visbal ran their simulation for more than 50,000 time steps on

Presented as Paper 0455 at the 44th AIAA Aerospace Sciences Meeting, Reno, NV, 9–12 January 2006; received 8 February 2006; revision received 2 November 2006; accepted for publication 29 November 2006.

*Research Associate Professor, Department of Mechanical Engineering. Senior Member AIAA.
†Senior Engineer. Senior Member AIAA.

254 processors using a second-order time, fourth-order spatial compact difference algorithm. No wall clock times were provided for the simulation. Although this simulation was useful for understanding the fluid dynamic phenomena of unsteady bay flow, it is presently too computationally expensive to apply to real flight vehicles.

This work investigates the level of fidelity of CFD required for simulating the flow inside a weapons bay in terms of both acoustics and time-averaged flowfield predictions. The CFD techniques examined include unsteady Euler, unsteady laminar, unsteady RANS with a turbulence model applied only to the upstream plate, unsteady RANS, and unsteady hybrid RANS/LES simulations. The objective was to determine if the reduced fidelity (and less expensive) CFD simulations could provide an adequate engineering estimate of the flow inside the bay for weapons separation investigations.

Approach

Computations were performed using the NXAIR [12] structured-grid overset Navier–Stokes solvers. NXAIR was run using second-order time with the third-order upwind HLLEM [19] flux algorithm. Steger–Warming flux vector splitting [20] was used for the inviscid flux Jacobians. Three Newton subiterations were used to provide local convergence at each time step. A symmetric successive overrelaxation (SSOR) procedure was used to solve the unfactored solution matrix. The turbulence transport equation was solved in a time accurate manner using a second-order time, second-order upwind space algorithm. The turbulence equation was solved in a loosely coupled manner with the mean flow equations within the Newton subiteration loop. The accuracy of NXAIR for unsteady flow applications is discussed in [21]. The wall function boundary condition of Nichols and Nelson [22] was used in the viscous NXAIR calculations.

The following unsteady flow physics approximations were evaluated:

1) Euler flow with slip walls everywhere;

2) Navier–Stokes with laminar flow everywhere;

3) Navier–Stokes with Baldwin–Lomax (BL) [9] turbulence model used on the upper plate only;

4) Navier–Stokes with the Spalart–Allmaras (SA) [23] one-equation transport turbulence model;

5) Navier–Stokes with the Spalart–Allmaras detached eddy simulation (SA-DES) [24] hybrid turbulence model.

The Euler flow represents the most simplified approach to this problem. The laminar flow and the BL approach are similar. Differences in these two models show the effect of simulating the upstream boundary layer. The BL and SA-DES can be considered hybrid RANS/LES approaches because both techniques attempt to apply RANS in the boundary layer and turn off the turbulence model outside of the boundary layer. The difference in these two techniques is that the BL approach limits the turbulence model to the upstream boundary layer only while SA-DES attempts to limit the turbulence outside the boundary layer based on local grid size.

The grid spacing, time step, and convergence criteria developed in [17] was used in this study. Numerical convergence must be evaluated in a statistical sense for these unsteady flow simulations. Nichols [17] assumed that demonstrating that a solution is statistically stationary is a sufficient condition for demonstrating convergence. The unsteady computational output is evaluated using overlapping data windows. The windows are overlapped because of the limited number of samples available. The window overlap was chosen as 50% in this study.

Results

The length to diameter ratio (L/D) of 4.5 and 9.0 weapons internal carriage and separation (WICS) [15] bay geometries were examined in this effort. The WICS $L/D = 4.5$ bay geometry is considered a deep bay (the shear layer does not impinge on the ceiling of the bay). Deep bay geometries have received a great deal of attention both experimentally and computationally in the past. The WICS $L/D = 9.0$ bay geometry is a transitional bay (the shear layer attaches to the bay ceiling near the aft wall). Transitional and shallow bays have not been studied in detail computationally.

Unsteady computations for the WICS bays were performed for $M = 0.95$ and $Re = 2.5 \times 10^6$/ft. The $L/D = 4.5$ weapons bay was 18 in. long, 4 in. wide, and 4 in. deep, while the $L/D = 9.0$ bay was 18 in. long, 4 in. wide, and 2 in. deep. The bays were located behind a 15 in. flat plate in the experimental configuration. The computational geometry was a flat plate that extended 15 in. upstream of the bay to match the experimental geometry and 25 in. downstream of the bay. The sides of the computational grid extended 50 in. on either side of the bay centerline. The wall spacing was chosen as 0.0075 in., which corresponds to a y^+ of 50 on the upstream plate. The wall spacing inside the bay was set to 0.075 in. The larger wall spacing may be used inside the bay because the wall shear stress is much lower there. The entire computational grid for the $L/D = 4.5$ bay had 1.1×10^6 points, and 1.2×10^5 points were used to discretize the bay. The entire computational grid for the $L/D = 9.0$ bay had 9.4×10^5 points, and 1.7×10^5 points were used to discretize the bay. All calculations were performed using the 1.6×10^{-5} second time step that was shown to be adequate for time accuracy in [17].

Spectral results for the K18 transducer locations are presented for both bays. K18 is located on the bay back wall centerline 0.725 in. from the bay opening. The calculations were run 12,000 iterations and the final 8192 time steps were statistically analyzed. Seven data windows of 2048 samples were averaged to produce the spectra that are presented. The error in the overall sound pressure level (OASPL) (defined as the difference of the individual window result and the averaged result divided by the averaged result) was less than 1% for all results.

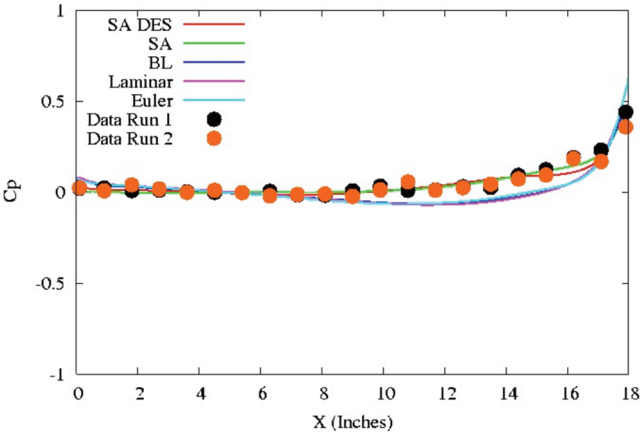

Fig. 1 Time-averaged pressure coefficient on the WICS $L/D = 4.5$ ceiling centerline.

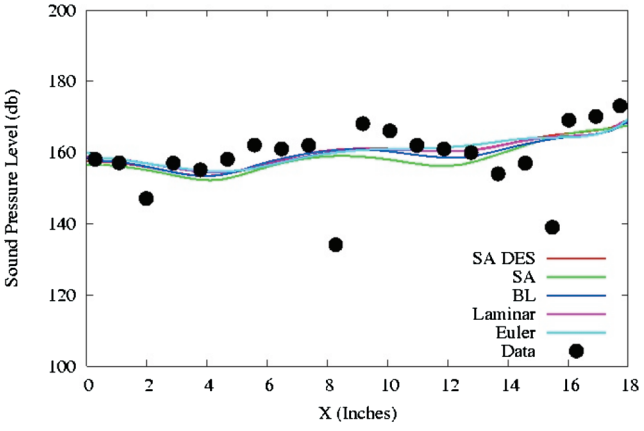

Fig. 2 Overall sound pressure level on the WICS $L/D = 4.5$ ceiling centerline.

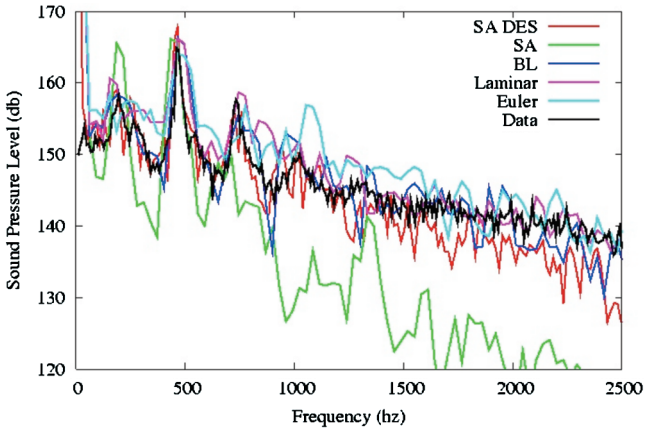

Fig. 3 Sound pressure level spectral results for the K18 location in the WICS $L/D = 4.5$ bay.

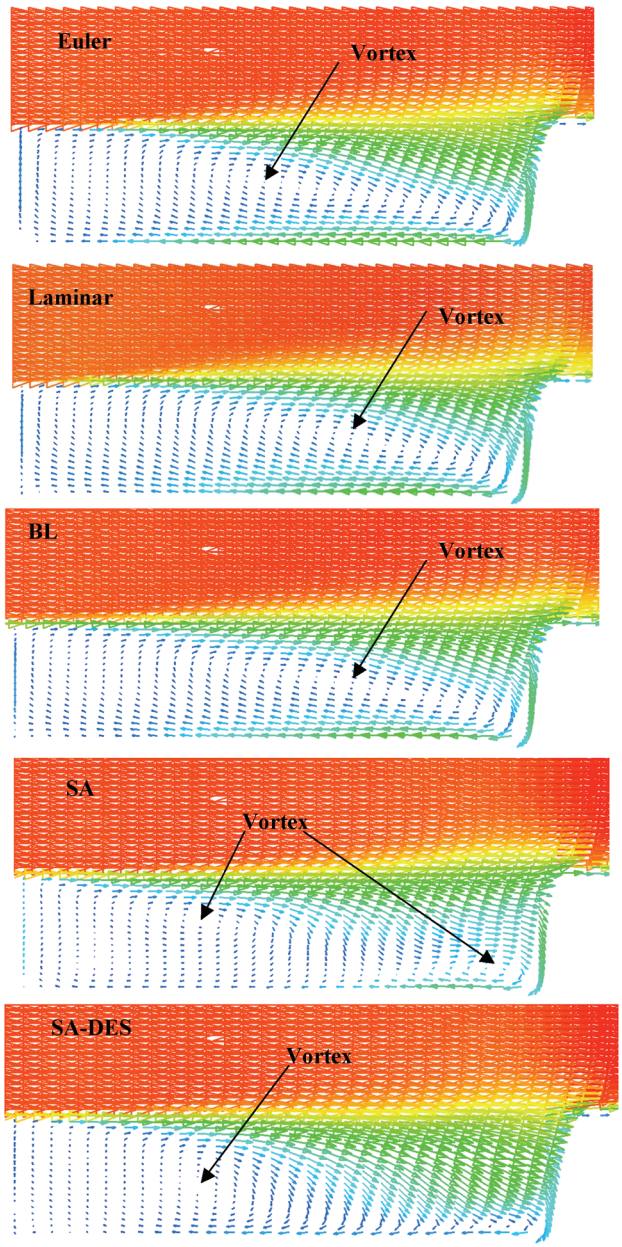

Fig. 4 Time-averaged velocity vectors colored by the Mach number on the centerline of the WICS $L/D = 4.5$ bay.

WICS $L/D = 4.5$

The time-averaged pressure coefficient on the WICS bay ceiling is shown in Fig. 1. All of the approximations are in reasonable agreement with the data. The Euler, laminar, and BL results are very similar and not in quite as good agreement with the data as the SA and SA-DES models. The OASPL on the ceiling is shown in Fig. 2. Again all of the approximations are in reasonable agreement with the data, with the SA model producing slightly lower results. Spectral results for the K18 transducer are shown in Fig. 3. The Euler, laminar, BL, and SA-DES results are in good agreement with the data for the first three spectral peaks. The Euler and laminar results are generally higher than the data. This is probably because the incoming boundary layer is not properly simulated. The SA result indicates that the unsteady flow is overdamped by the RANS approximation of the turbulent flow.

Time-averaged velocity vectors colored by the Mach number on the center plane of the cavity are shown in Fig. 4. The vectors were interpolated onto a Cartesian grid for clarity and do not represent the computational mesh system. The Euler, laminar, and BL solutions are very similar with all showing a single large vortex in the bay that produces a high-speed region near the aft wall and the ceiling. The SA solution shows two vortices in the bay. The SA solution has lower velocity and flow angles in the aft-upper portion of the bay than predicted by the Euler, laminar, and BL approximations. The SA-DES solution has a large vortex in the bay. The high-speed region in the SA-DES solution is larger in the aft-upper portion of the bay than predicted by the Euler, laminar, and BL solutions. Time-averaged velocity vectors colored by the Mach number are shown on a crossflow plane located 10 in. behind the aft wall of the cavity in Fig. 5. None of the models produce perfectly symmetrical flow from averaging just 8192 samples in time. The laminar, SA, and BL solutions are particularly unsymmetrical. The Euler solution predicts a large pair of symmetric vortices in the upper part of the bay and a weaker set of counterrotating vortices in the bottom of the bay. The SA-DES solution shows a pair of symmetric vortices that are much

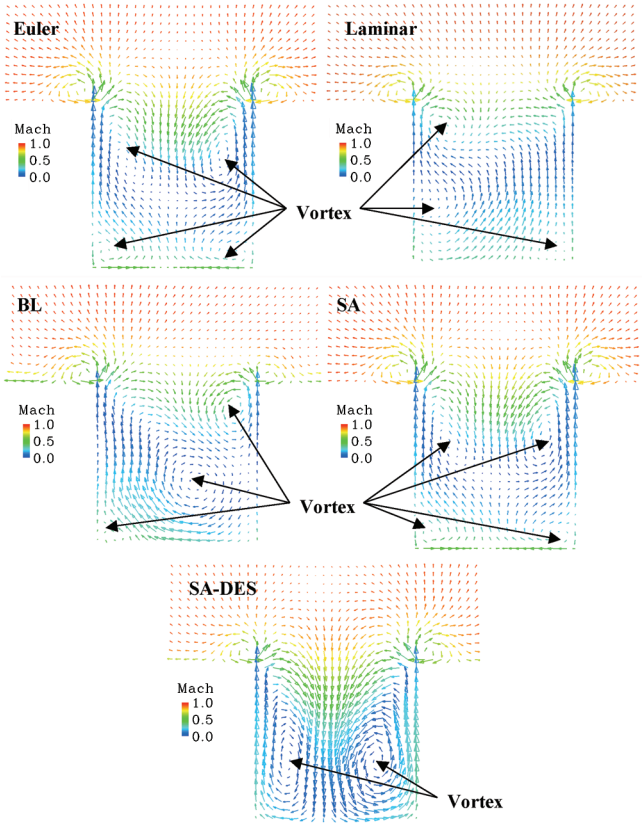

Fig. 5 Time-averaged velocity vectors colored by the Mach number at $x = 10$ in. for the WICS $L/D = 4.5$ bay.

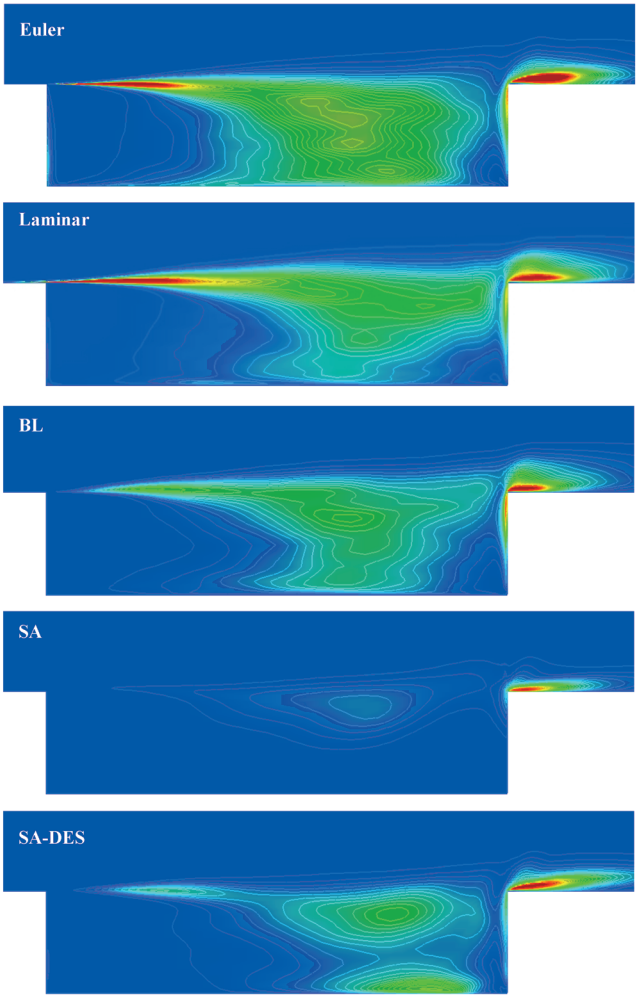

Fig. 6 Time-averaged grid-realized turbulent kinetic energy for the centerline of the WICS $L/D = 4.5$ bay.

stronger and lower in the bay than the vortices predicted by the other approximations.

Time-averaged grid-realized turbulent kinetic energy (TKE) on the bay centerline is shown in Fig. 6. This provides an indication of where the unsteady flow occurs and the degree of unsteadiness present. The Euler and laminar solutions show much higher values of TKE in the initial shear layer than do the other approaches. This is due to the improper simulation of the incoming boundary layer. The Euler, laminar, and BL solutions also have much higher TKE levels in the aft half of the bay than does the SA-DES model. This indicates

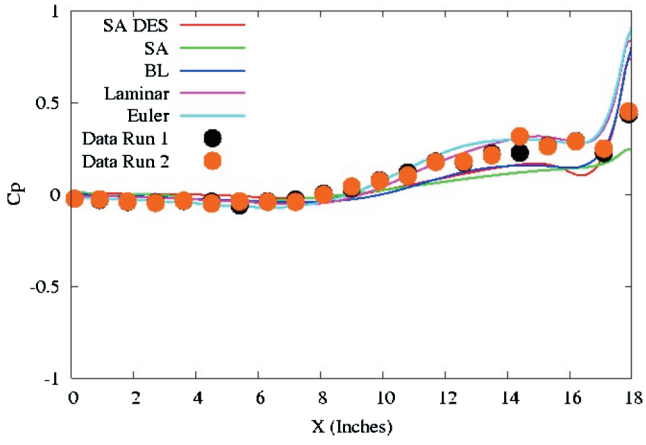

Fig. 7 Time-averaged pressure coefficient on the WICS $L/D = 9.0$ ceiling centerline.

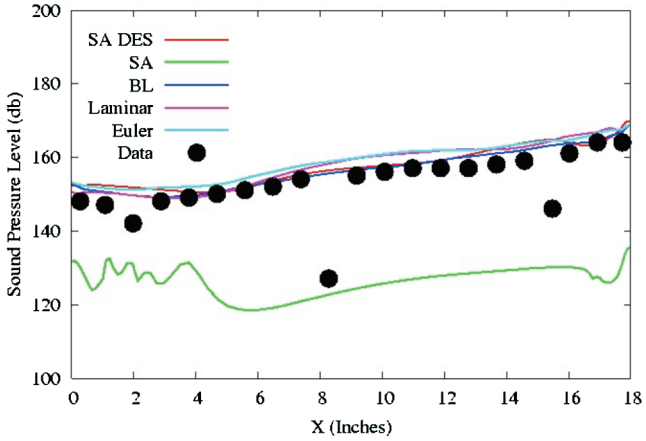

Fig. 8 Overall sound pressure level on the WICS $L/D = 9.0$ ceiling centerline.

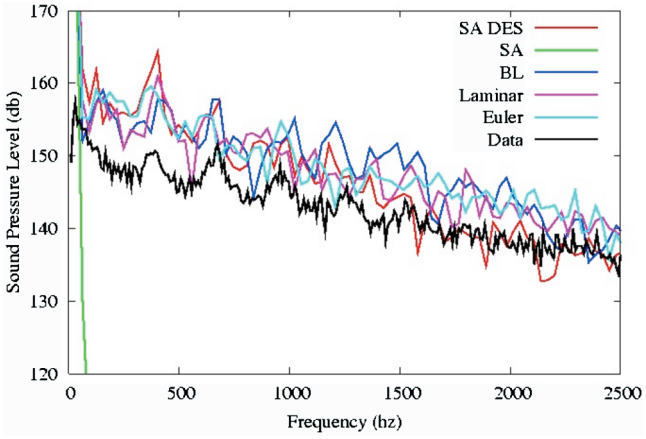

Fig. 9 Sound pressure level spectral results for the K18 location in the WICS $L/D = 9.0$ bay.

that the SA-DES model is providing some turbulent damping in the bay. The RANS SA model allows very little unsteady flow to occur.

WICS $L/D = 9.0$

The time-averaged pressure coefficient on the WICS bay ceiling is shown in Fig. 7. All of the approximations are in reasonable agreement with the data. The Euler and laminar solutions are similar to each other, and the BL and SA-DES solutions are also similar to each other. The SA solution has a different character from the other approximations. The SA model underpredicts the pressure coefficient at the aft wall while the other models overpredict the pressure coefficient there. The OASPL on the ceiling is shown in Fig. 8. The Euler, laminar, BL, and SA-DES results lie slightly above the data with the Euler results having the highest OASPL. The SA results lie well below the data, indicating that the SA model produces an almost steady-state solution. Spectral results for the K18 transducer location are shown in Fig. 9. The SA solution was essentially steady state, so the spectrum for SA falls well below the plot scale in Fig. 9.

Time-averaged velocity vectors colored by the Mach number on the center plane of the cavity are shown in Fig. 10. The vectors were interpolated onto a Cartesian grid for clarity and do not represent the computational mesh system. The Euler, laminar, BL, and SA-DES solutions are very similar with all showing a single large vortex in the bay. The Euler solution has higher velocities near the bay ceiling because of the no-slip wall. The SA solution has a single strong vortex in the bay and a thinner shear layer in the aft part of the bay than the other solutions. Time-averaged velocity vectors colored by the Mach number are shown on a streamwise plane located 10 in. behind the start of the cavity in Fig. 11. None of the models produce

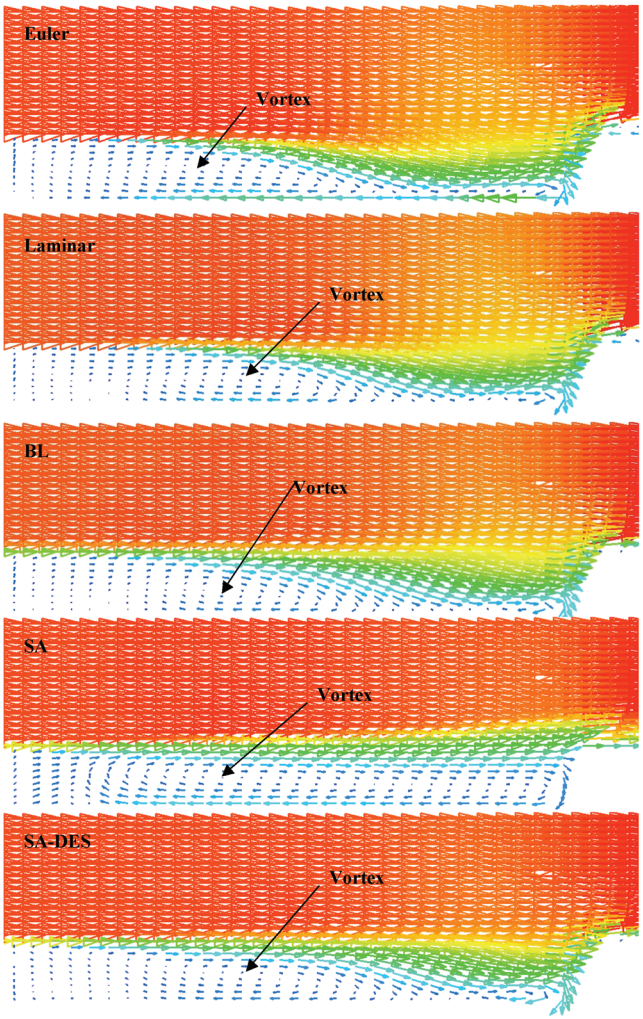

Fig. 10 Time-averaged velocity vectors colored by the Mach number on the centerline of the WICS $L/D = 9.0$ bay.

perfectly symmetrical flow from averaging just 8192 samples in time. The Euler, laminar, BL, and SA-DES solutions are similar in that they both predict a large pair of symmetric vortices. The vortices predicted by the SA-DES model are weaker and lower in the bay than

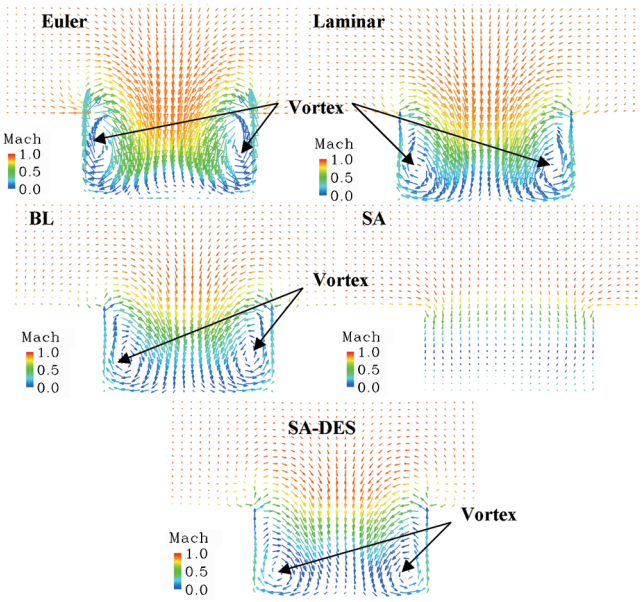

Fig. 11 Time-averaged velocity vectors colored by the Mach number at $x = 10$ in. for the WICS $L/D = 9.0$ bay.

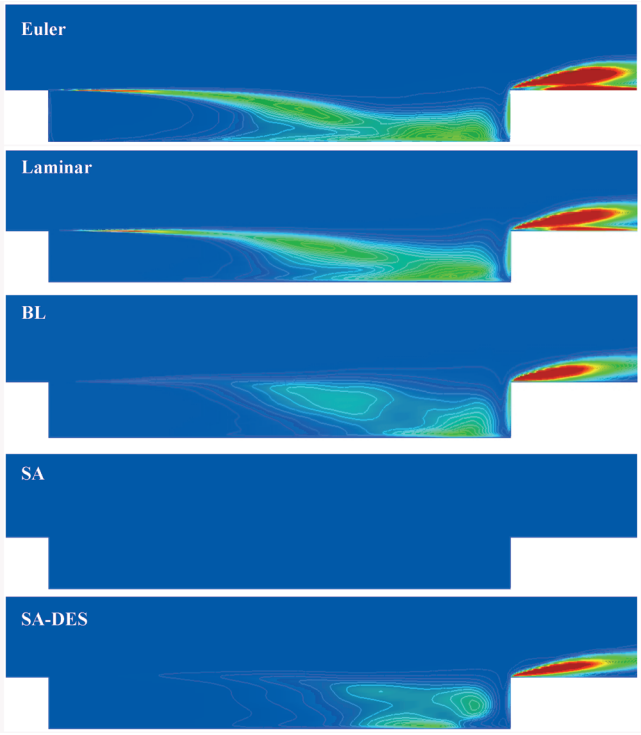

Fig. 12 Time-averaged grid-realized turbulent kinetic energy for the centerline of the WICS $L/D = 9.0$ bay.

those predicted by the Euler, laminar, and BL approximations. The SA solution shows almost no crossflow velocity.

Time-averaged grid-realized TKE on the bay centerline is shown in Fig. 12. The Euler and laminar solutions show high values of TKE in the initial shear layer than do the other approaches. The Euler and laminar solutions also have much higher TKE levels in the aft half of the bay than do the BL or SA-DES models. The differences in the Euler and laminar solutions and the BL and SA-DES solutions are due to the improper simulation of the incoming boundary layer. The RANS SA model allows almost no unsteady flow to occur.

Conclusions

Five approximations to the Navier–Stokes equations have been used to simulate the flow inside a weapons bay: the Euler equations, laminar flow everywhere, Baldwin–Lomax applied only to the upstream plate, unsteady RANS with a transport turbulence model, and Navier–Stokes equations with hybrid RANS/LES turbulence models for bay flow simulations. Calculations were performed on the WICS $L/D = 4.5$ deep bay and the WICS $L/D = 9.0$ transitional bay.

All of the simulation techniques produced reasonable results for the WICS $L/D = 4.5$ deep bay for time-averaged pressure and sound surface quantities. All but the SA model were adequate at predicting the frequencies of the first three unsteady modes of the surface pressure. All models overpredicted the acoustic intensity of the first mode.

The SA RANS model produced an almost steady solution for the WICS $L/D = 9.0$ bay. All of the other simulation techniques overpredicted the unsteady flow surface pressure quantities for the WICS $L/D = 9.0$ shallow bay. The proper solution seems to lie somewhere between the SA and SA-DES results, indicating that the hybrid model is transitioning from RANS to LES too quickly for this case.

There seems to be little correlation between the surface pressure results and the time-averaged flow structure in either of the bays. The differences in the flow angularity between the models could have significant effects on the separation characteristics of a weapon from these bays. If the higher fidelity SA-DES results are accepted as the most accurate simulation approach, the other approximation techniques would have to be discounted for producing time-averaged

flowfields for weapons separation evaluations. These results also indicate that validation against surface acoustic data alone is not sufficient for assuring that time-averaged flowfield quantities will be faithfully reproduced in a bay configuration. Thus time-averaged flow data in bay geometries is needed for CFD validation.

Acknowledgments

This work was made possible through support provided by the DoD High Performance Computing Modernization Program (HPCMP) and Productivity Enhancement and Technology Transfer (PET) activities through Mississippi State University under terms of Contract No. N62306-01-D-7110.

References

[1] Baker, W., Keen, S., and Morgret, C., "Validation of Weapon Separation Predictions Using F/A-22 Flight Test Results," AIAA Paper 2004-6803, Nov. 2004.

[2] Keen, K. S., "New Approaches to Computational Aircraft/Store Weapons Integration," AIAA Paper 90-0274, Jan. 1990.

[3] Lee, J. M., Dunworth, K. S., Rizk, M., Westmoreland, W. S., and Atkins, D. J., "Studies of Combined Use of CFD and Wind Tunnel Test Approaches to Simulate a Store Separation from F-15E Using Efficient CFD Database Generation," AIAA Paper 2004-4724, Aug. 2004.

[4] Dunworth, K. S., Atkins, D. J., and Lee, J. M., "Incorporation of CFD Generated Aerodynamic Data in Store Separation Predictions," AIAA Paper 2005-846, Jan. 2005.

[5] Jordan, J. K., and Denny, A. G., "Approximation Methods for Computational Trajectory Predictions of a Store Released from a Bay," AIAA Paper 97-2201, July 1997.

[6] Rizzetta, D. P., "Numerical Simulation of Supersonic Flow over a Three Dimensional Cavity," *AIAA Journal*, Vol. 26, No. 7, 1988, pp. 799–807.

[7] Suhs, N. E., "Computations of Three Dimensional Cavity Flow at Subsonic and Supersonic Mach Numbers," AEDC TR-88-30, 1988.

[8] Baysal, O., Yen, G. W., and Fouladi, K., "Navier-Stokes Computations of Cavity Aeroacoustics with Suppression Devices," AIAA/DGLR Paper 92-02-161, May 1992.

[9] Baldwin, B. S., and Lomax, H., "Thin Layer Approximation and Algebraic Model for Separated Turbulent Flows," AIAA Paper 78-0257, Jan. 1978.

[10] Atwood, C. A., "Computation of a Controlled Store Separation from a Cavity," AIAA Paper 94-0031, Jan. 1994.

[11] Welterlen, T. J., "Weapons Bay Flow Field Simulation," AIAA Paper 2000-3926, Aug. 2000.

[12] Tramel, R. W., and Nichols, R. H., "A Highly Efficient Numerical Method for Overset-Mesh Moving–Body Problems," AIAA Paper 97-2040, June 1997.

[13] Sinha, N., Dash, S., Chidambaram, N., and Findlay, D., "A Perspective on the Simulation of Cavity Aeroacoustics," AIAA Paper 98-0286, Jan. 1998.

[14] Arunajatesan, S., Shipman, J. D., and Sinha, N., "Hybrid RANS-LES Simulation of Cavity Flow Fields with Control," AIAA Paper 2002-1130, Jan. 2002.

[15] Dix, R. E., and Bauer, R. C., "Experimental and Theoretical Study of Cavity Acoustics," AEDC TR-99-4, May 2000.

[16] Nichols, R. H., and Nelson, C. C., "Application of Hybrid RANS/LES Turbulence Models," AIAA Paper 2003-0083, Jan. 2003.

[17] Nichols, R. H., "Comparison of Hybrid RANS/LES Turbulence Models for a Circular Cylinder and a Generic Weapons Bay," *AIAA Journal*, Vol. 44, No. 6, 2006, pp. 1207–1219.

[18] Rizzetta, D. P., and Visbal, M. R., "Large-Eddy Simulation of Supersonic Cavity Flowfields Including Flow Control," AIAA Paper 2002-2853, June 2002.

[19] Einfeldt, B., Munz, C. D., Roe, P. L., and Sjogreen, B., "On Godunov-Type Methods Near Low Densities," *Journal of Computational Physics*, Vol. 92, No. 2, 1991, pp. 273–295.

[20] Steger, J. L., and Warming, R. F., "Flux Vector Splitting of the Inviscid Gasdynamic Equations with Application to Finite-Difference Methods," *Journal of Computational Physics*, Vol. 40, April 1981, pp. 263–293.

[21] Nichols, R. H., and Heikkinen, B. D., "Validation of Implicit Algorithms for Unsteady Flows Including Moving and Deforming Grids," *Journal of Aircraft*, Vol. 43, No. 5, Sept. 2006, pp. 1341–1351.

[22] Nichols, R. H., and Nelson, C. C., "Wall Function Boundary Conditions Including Heat Transfer and Compressibility," *AIAA Journal*, Vol. 42, No. 6, June 2004, pp. 1107–1114.

[23] Spalart, P. R., and Allmaras, S. R., "A One-Equation Turbulence Model for Aerodynamic Flows," AIAA Paper 92-0439, Jan. 1992.

[24] Spalart, P., Jou, W.-H., Strelets, M., and Allmaras, S., "*Comments on the Feasibility of LES for Wings and on a Hybrid RANS/LES Approach*," edited by C. Liu and Z. Liu, Greyden Press, Columbus, OH, Aug. 1997.